Mon. Not. R. Astron. Soc. **286,** 785–794 (1997)

A jet–cloud interaction in 3C 34 at redshift $z = 0.69$

P. N. Best,[1,2] M. S. Longair[1] and H. J. A. Röttgering[2]

[1] *Cavendish Laboratory, Madingley Road, Cambridge CB3 0HE*

[2] *Sterrewacht Leiden, Huygens Laboratory, PO Box 9513, 2300 RA Leiden, The Netherlands*

Accepted 1996 October 11. Received 1996 September 5; in original form 1996 May 29

ABSTRACT

We report the detection of a strong jet–cloud interaction at a distance of 120 kpc from the nucleus of the radio galaxy 3C 34, which has redshift $z = 0.69$. *Hubble Space Telescope* images of the radio galaxy show a long narrow region of blue emission orientated along the radio axis and directed towards a radio hotspot. The William Herschel Telescope has been used to provide long-slit spectroscopic data of this object, and infrared observations made with the United Kingdom InfraRed Telescope have enabled its spectral energy distribution to be modelled. We propose that the aligned emission is associated with a region of massive star formation, induced by the passage of the radio jet through a galaxy within the cluster surrounding 3C 34. A star formation rate of about $100\,M_{\odot}\ yr^{-1}$ is required, similar to the values necessary to produce the alignment effect in high-redshift radio galaxies. The consequences of this result for models of star formation in distant radio galaxies are discussed.

Key words: galaxies: active – galaxies: individual: 3C 34 – galaxies: starburst – infrared: galaxies – radio continuum: galaxies.

1 INTRODUCTION

In 1985 it was discovered that the optical colours and line ratios of Minkowski's object, a peculiar galaxy lying along the radio jet of the source PKS 0123–016 at redshift $z = 0.019$, are consistent with it recently having undergone a period of intense star formation (Brodie, Bowyer & McCarthy 1985; van Breugel et al. 1985). This was interpreted as having been triggered by the interaction of the radio jet with a gas-rich cloud along its path. Similar phenomena have also been observed in other low-redshift galaxies, most notably in the lobe of the double radio source 3C 285 ($z = 0.0794$, van Breugel & Dey 1993).

In 1987, Chambers et al. and McCarthy et al. discovered that the optical emission of powerful radio galaxies at redshift $z \gtrsim 0.6$ is elongated and aligned along the radio axis. A natural interpretation of these aligned blue structures was to associate them with regions of massive star formation induced by shocks associated with the passage of the radio jet (e.g. Rees 1989). However, despite various theoretical works suggesting that powerful jets in these high-redshift sources are capable of producing the observed levels of bright aligned structures (De Young 1989; Begelman & Cioffi 1989; Daly 1990), direct evidence for the presence of young stars has been scarce. Indeed, the discovery that the extended optical emission is frequently polarized [e.g. Dey & Spinrad (1996) and references therein] indicates that at least a proportion of the aligned light must be associated with light scattered from an obscured active nucleus.

We are undertaking an investigation of an almost complete sample of 28 radio galaxies with redshifts $0.6 < z < 1.8$ from the 3CR catalogue of Laing, Riley & Longair (1983). In this paper, we discuss the case of the radio galaxy 3C 34, which is a typical FRII double radio source (Fanaroff & Riley 1974) whose host galaxy is the brightest member of a rich compact cluster of galaxies (McCarthy 1988) at redshift $z = 0.689$. *Hubble Space Telescope* observations provide evidence for a jet–cloud interaction having occurred in this radio source, the cloud in this case being associated with the interstellar gas of a galaxy within the cluster.

The observations are presented in Section 2, together with details of the data reduction. In Section 3, we discuss the evidence for a jet–cloud interaction having occurred in this radio source. We consider the various causes of the observed optical alignment in Section 4, and show that the observations are consistent with jet-induced star formation models. Our conclusions are presented in Section 5.

2 OBSERVATIONS

The field of 3C 34 was imaged using the Wide-Field Planetary Camera II (WFPC2) of the *Hubble Space Telescope* (*HST*) for 1700 s through each of the two filters f555W and f785LP, centred at wavelengths of 545 and 865 nm and corresponding to rest-frame near-ultraviolet and visible wavelengths respectively. The data were reduced according to the standard Space Telescope Science Institute pipeline (Lauer 1989). Radio data with comparable angular resolution to the *HST* images were obtained using the Very Large Array radio interferometer (VLA) at 8.4 GHz, for 44 min in the A-array configuration and 30 min using the C-array. The AIPS software provided by the National Radio Astronomy Observatory was used to reduce these data (Perley 1989). In addition, the field was observed in each of the infrared J (1.2 μm)

and K (2.2 μm) wavebands using UKIRT for 54 min, in 1994 August. The reader is referred to Best, Longair & Röttgering (1997) for a full discussion of the data reduction.

Fig. 1(a) (opposite p. 786) shows the *HST* image of the galaxy as observed through the f555W filter, with the radio contours from the A-array observations overlaid. In Fig. 1(b) we present a deep 4.8-GHz radio map (provided courtesy of Dr J.P. Leahy) overlaid upon the *HST* image through the f785LP filter. Of particular interest is the emission feature, hereafter object 'a', at RA 01^{h} 10^{m} $17\overset{s}{.}3$, Dec. 31° 47′ 18″ (J2000): two long, narrow regions of intense blue emission lie directly along a line from the radio core to the northern of the pair of radio hotspots in the western lobe (hotspot 'n'). A further emission knot lies just to the south of these. In Fig. 2 (opposite p. 786) we present enlarged images of object 'a' at all four wavelengths to show the wavelength-dependent morphology of this region. For comparison, in Fig. 3 (opposite p. 786) we present enlarged images of the host radio galaxy 3C 34 on the same angular scale, and with the same grey-scale levels.

Object 'a' lies 15 arcsec from the host galaxy 3C 34, corresponding to a projected distance of 120 kpc, assuming $H_0 = 50\,\mathrm{km\ s^{-1}\ Mpc^{-1}}$ and $\Omega = 1$. The large length-to-width extension along the radio axis of these optical emission regions strongly suggests an association with the radio source, and that they are produced by an interaction of the radio jet powering the outer hotspots with a cloud of ambient gas, rather than by a beam of ionizing photons from an obscured quasar nucleus.

In 1995 December a long-slit spectrum of this source was obtained using the ISIS spectrograph on the William Herschel Telescope (WHT). A slit of width 2.5 arcsec was orientated at position angle $86\overset{\circ}{.}5$, containing both the host radio galaxy and object 'a'. The R158R and R158B gratings were used in the red and blue arms of the spectrograph respectively, in conjunction with TEK CCDs. Since only a short (900 s) observation was made, the read-noise was reduced by binning the data into pixel pairs in the wavelength direction. The total useful wavelength range of the two ISIS arms was about 3500 to 8500 Å, with a small gap from 5700 to 6000 Å. The effective spectral resolution FWHM was 6 Å, and the seeing was about 1 arcsec. The standard star SP0105+625 was observed immediately before 3C 34 to provide accurate flux calibration, whilst wavelength calibration was obtained by observations of a Cu–Ar arc lamp. The spectra were reduced using standard IRAF routines.

The spectrum of object 'a' is presented in Fig. 4(a). It can be seen that this shows no evidence of any line emission, making it impossible to derive a redshift for the source. Line emission of both [O II] 3727 and [O III] 5007 at a redshift of 0.689 would fall within this spectrum. For comparison, in Fig. 4(b) we present the spectrum of the host radio galaxy 3C 34, which also lay within the slit. These strong emission lines dominate this spectrum, with flux densities of $f_{[\mathrm{O\,II}]\,3727} = (9.7 \pm 0.3) \times 10^{-19}\,\mathrm{W\,m^{-2}}$ and $f_{[\mathrm{O\,III}]\,5007} = (15.1 \pm 0.6) \times 10^{-19}\,\mathrm{W\,m^{-2}}$.

The broad-band flux densities[1] from the two *HST* images are marked on each spectrum. These were obtained by convolving the *HST* images to a resolution comparable to the seeing of the spectroscopic data, and then extracting the flux densities through apertures of the same size and shape as the slit. For 3C 34, the broad-band *HST* flux densities were corrected for line contamination, using line fluxes measured from the spectral data (taking into account the misplacement of the slit – see below), thus providing an estimate of the continuum flux density alone. It can be seen that, for both spectra, these flux densities are almost a factor of 2 greater than the values predicted from the spectrum, although the colour of the spectrum matches the broad-band *HST* colours. Since this is true of the spectra of both sources, the most likely explanation is that the slit was misplaced from the centre of the targets by about 1.0 arcsec.

The dashed lines in Fig. 4 represent the spectral energy distributions (SEDs) derived in Section 3.3 from stellar synthesis fits to the broad-band flux densities, and normalized to match the observed spectra. The spectral energy distribution derived for 3C 34 provides a good match apart from the strong emission lines, which are excited by photoionization from the nucleus. Although the observed galaxy 'a' spectrum is dominated by noise, it is consistent with the overall shape of the fitted SED, including the 4000-Å break.

3 AN EMISSION KNOT ON THE RADIO AXIS?

3.1 Evidence from the radio properties

The radio image of 3C 34 (Fig. 1b) indicates the possible presence of radio jets in both lobes of the radio source. Garrington, Conway & Leahy (1991) and Johnson et al. (1995) have interpreted the two knots within the eastern lobe as being associated with the radio jet; they have flatter spectral indices than the surrounding lobe material, and the magnetic field is aligned along the direction to the core, characteristic of radio jets in FRII sources. Directly opposite these, the western arm shows an extension from the core and two slightly enhanced regions of radio emission along a line towards the more southerly of the two radio hotspots (hotspot 's'). Many pieces of evidence indicate that hotspot 's' is the current primary hotspot in the western lobe: (i) the present axis of the radio jets, as defined by the radio knots and the western nuclear radio jet, is oriented towards this hotspot; (ii) the 8.4-GHz A-array observations (Fig. 1a) show that it is the more compact of the two western hotspots; (iii) the 1.4–4.8 GHz spectral indices of hotspots 's' and 'n' are 0.83 ± 0.03 and 0.92 ± 0.03 respectively, the flatter spectral index of hotspot 's' indicating that it is younger; for comparison the spectral index of the eastern 'hotspot' is 0.82 ± 0.03.

The jet therefore appears to be currently pointing towards hotspot 's', and not passing through object 'a'. Given this, we must consider the nature of hotspot 'n'. Is it the site of an old impact of a precessing jet (Scheuer 1982), which at one time passed along the line through object 'a', or is it a 'splatter-spot' where material flowing out of the primary hotspot 's' strikes the opposite side of the radio cocoon (Williams & Gull 1985)? The former hypothesis is supported by evidence for precession of the jet in the eastern lobe of the source: the A-array data (Fig. 1a) show that the emission from the end of the eastern lobe is confused, with evidence for at least two hotspots; in addition, the current jet direction in the eastern lobe, as defined by the two knots of emission, points directly along the line from the active hotspot 's' in the western lobe through the radio core, but does not point towards the eastern hotspots, consistent with precession of the jet.

Cox, Gull & Scheuer (1991) showed that if a jet is steadily precessing it initially makes a glancing impact upon the cocoon wall, causing it to curve round but continue to feed the same hotspot. As it precesses further, the jet eventually strikes the cocoon wall at a sharp enough angle to generate a new primary hotspot, upstream of the old primary. This is consistent with the

[1] Broad-band flux densities are obtained by assuming that the emission is flat across the filter, and are placed at the central filter wavelength. Errors in this approximation are comparable to or smaller than the other errors in measuring the flux densities.

Opposite p. 786, MNRAS, **286**

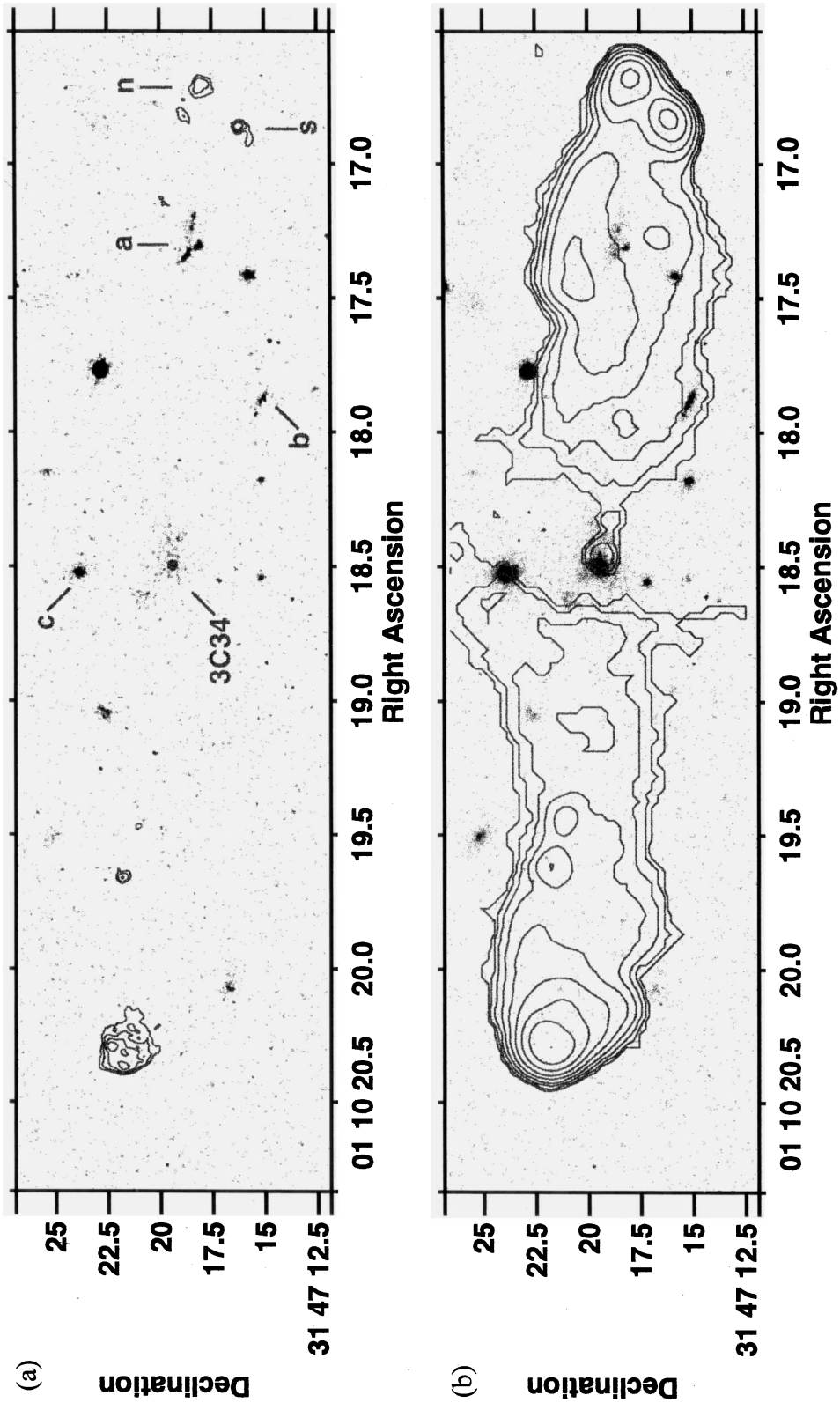

Figure 1. (a) (Top) An image of 3C 34 at 545 nm taken using the *Hubble Space Telescope*, with contours of the VLA A-array radio emission at 8.4 GHz overlaid. Contour levels are 120 μJy × (2, 4, 8, 16). (b) (Bottom) An *HST* image of 3C 34 at 865 nm, overlaid with contours of the radio emission at 4.8 GHz as seen using B- and C-arrays of the VLA (Johnson, Leahy & Garrington 1995). Contour levels are 120 μJy × (1, 2, 4, 8, 16, 32, 64, 128). All coordinates are measured in equinox J2000.

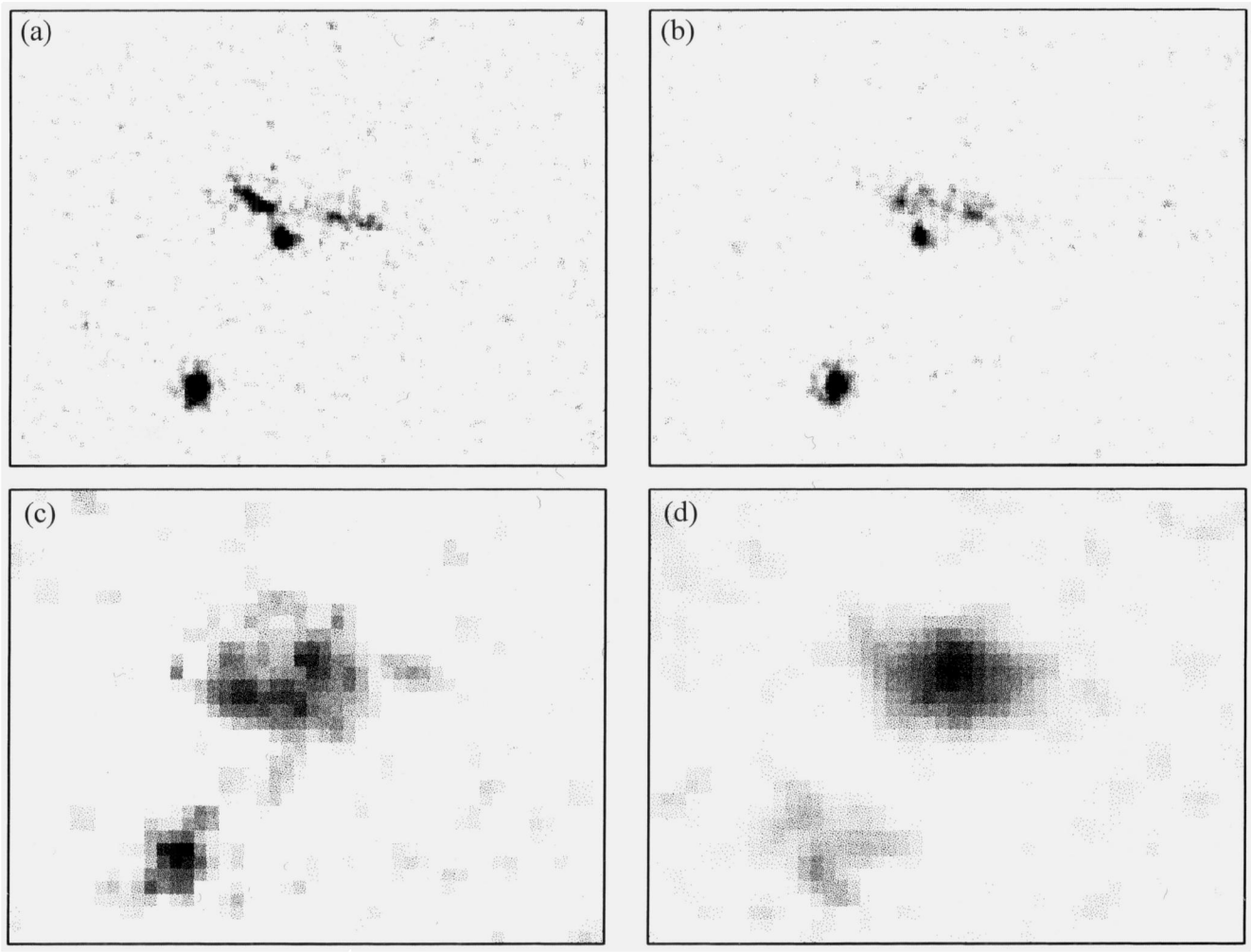

Figure 2. Enlarged images of object 'a': (a: upper left) *HST* image through f555W filter; (b: upper right) *HST* image through f785LP filter; (c: lower left) *J*-band (1.2 μm) UKIRT image; (d: lower right) *K*-band (2.2 μm) UKIRT image. All four images are 9.6 × 7.2 arcsec^2.

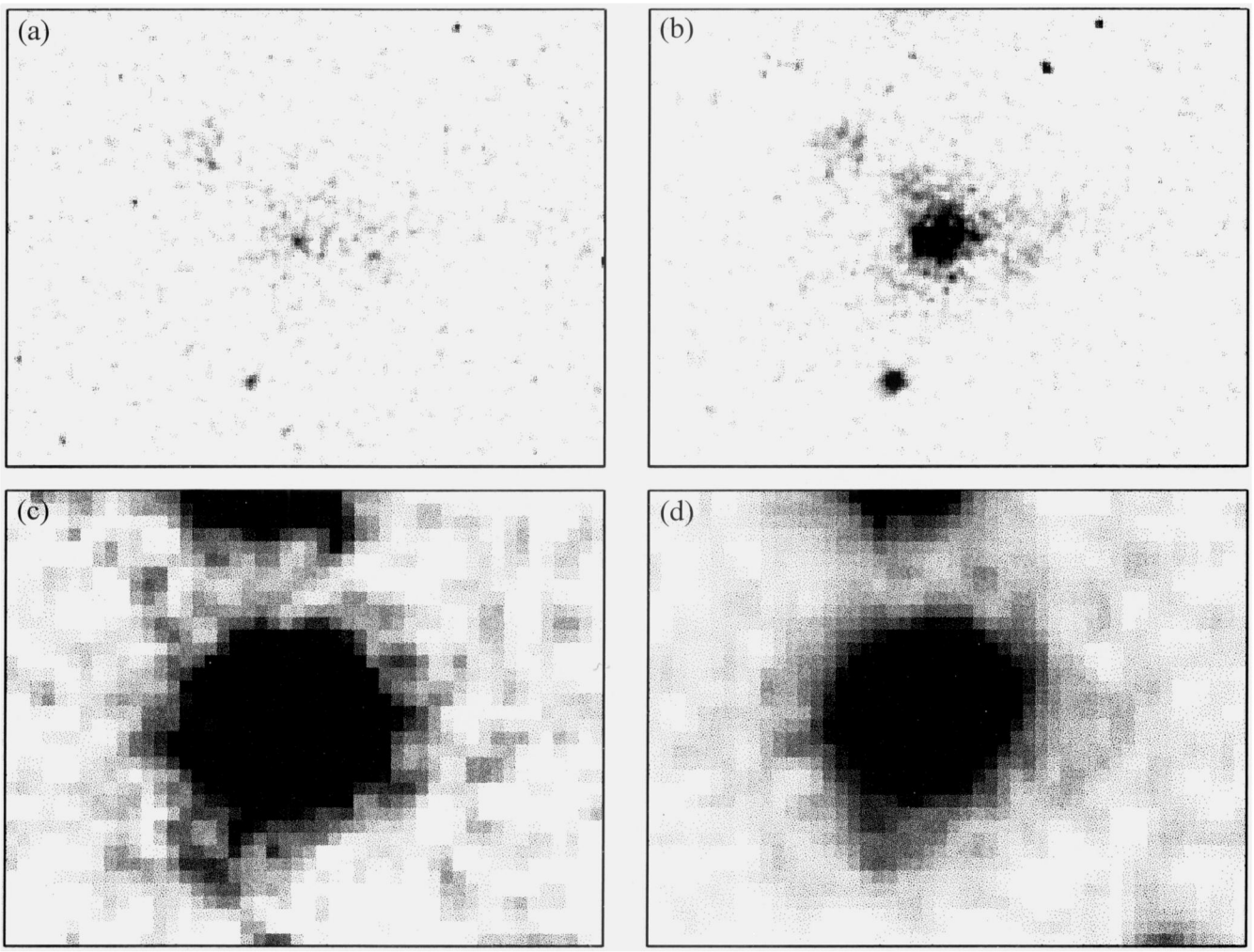

Figure 3. Enlarged images of the galaxy associated with 3C 34 in four wavebands: (a: upper left) *HST* image through f555W filter; (b: upper right) *HST* image through f785LP filter; (c: lower left) *J*-band (1.2 μm) UKIRT image; (d: lower right) *K*-band (2.2 μm) UKIRT image. Both angular sizes and grey-scale levels are the same as in Fig. 2.

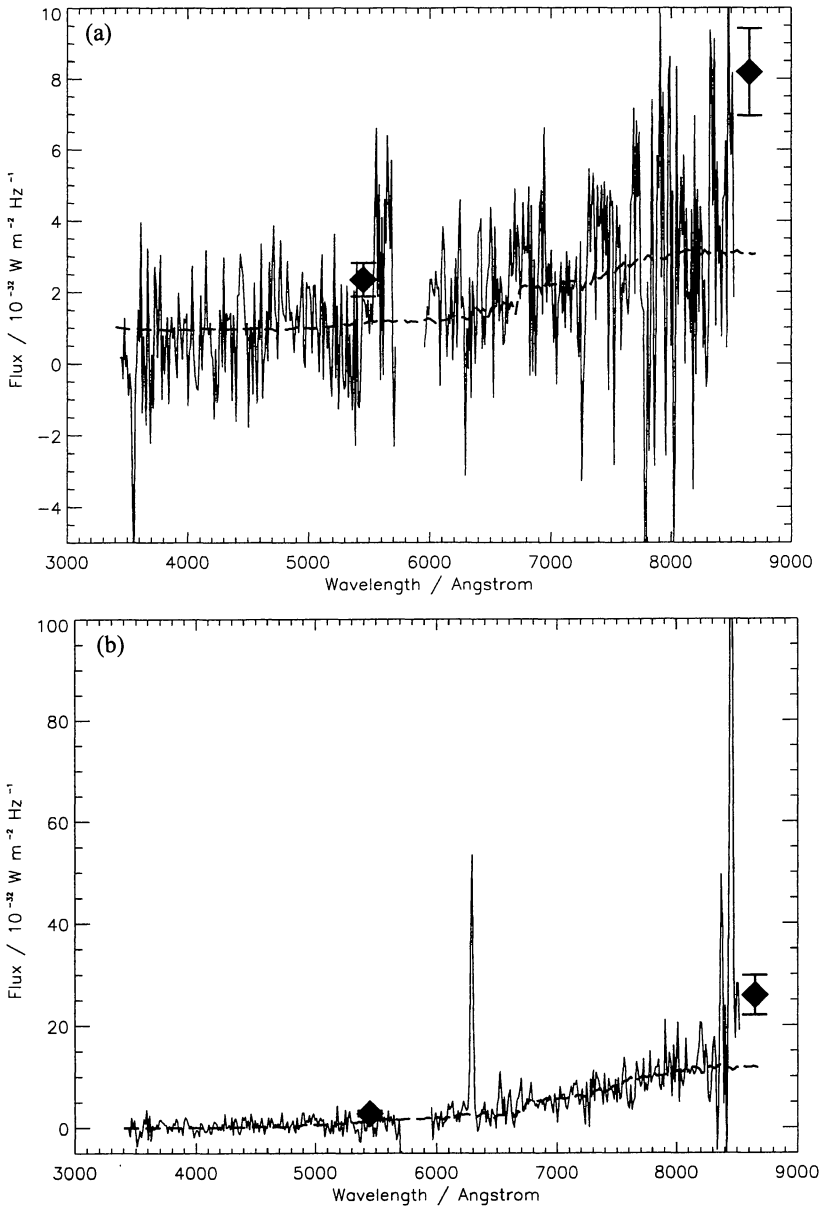

Figure 4. (a) (Top) A 900-s spectrum of object 'a' taken using the ISIS spectrograph on the WHT. Both red and blue arms are shown. (b) (Bottom) A spectrum of 3C 34, taken through the same long slit. In each case, the broad-band *HST* flux densities are marked by filled diamonds (for 3C 34 these have been corrected for line contamination, to give an estimate of the continuum flux density). These flux densities indicate that the slit did not pass through the centre of these objects – see text for more details. The dashed lines show the fits to the spectrum using the stellar synthesis models discussed in Section 3.3.

relative locations of hotspots 's' and 'n'. It could also explain the 'arc' of radio emission to the south of hotspot 's' in the A-array image; the jet may have precessed slightly beyond this hotspot but is still continuing to feed it. Note also that the angle of precession required for the jet to move from pointing towards hotspot 'n' to pointing towards hotspot 's' ($\lesssim 10°$) is comparable to the precession angles required to account for the observed asymmetries in powerful double radio sources (Best et al. 1995). It therefore seems likely that, at some previous time, the jet was pointing towards the hotspot 'n'.

Despite the unavailability of a redshift, there is strong circumstantial evidence that object 'a' is associated with the radio source, rather than merely being a foreground or background object along the line of sight. The deep radio map (Fig. 1b) shows an enhanced region of radio emission lying to the north of object 'a'. The radio spectral index of this region is not as steep as that of the rest of the radio lobe, and increases away from the hotspot, indicating a region of rapid backflow from the hotspot (Blundell 1994). This backflow loops around to the north of object 'a' rather than passing through it, consistent with object 'a' lying within the radio lobe, and the relativistic electrons flowing out from the hotspot avoiding this region of higher gas density.

The western lobe of this source has a higher Faraday depolarization than the eastern lobe, and high-resolution depolarization mapping by Johnson et al. (1995) has shown this to be associated with a 'depolarization silhouette' which lies directly at the position of object 'a'. The 21- to 6-cm depolarization measure (DP_6^{21}) is defined as the ratio of the percentage polarization at 21 cm to that at

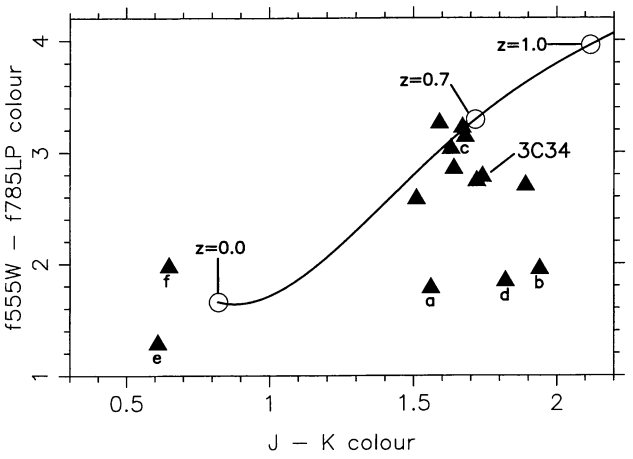

Figure 5. A plot of optical versus infrared colour for galaxies with $K < 19$ which lie within 250 kpc of the radio galaxy 3C 34. Galaxies are plotted as filled triangles, with typical errors of ± 0.2 in each coordinate. The solid line represents the colour track obtained by redshifting a standard, current-epoch giant elliptical galaxy. The open circular markers along this line indicate redshifts of 0.0, 0.7 and 1.0.

6 cm. In a 5 arcsec long region, with a pear-shaped morphology almost identical to that of object 'a', the depolarization measure has a value of $DP_6^{21} \lesssim 0.1$ to 0.2, as compared with that of the surrounding lobe of $DP_6^{21} \gtrsim 0.5$. Johnson et al. (1995) associate this depolarization with a cluster galaxy lying in front of the lobe, but it would also be consistent with object 'a' lying within the radio lobe.

3.2 Optical and infrared properties of the knot

In Fig. 5 we plot the f555W–f785LP colour[2] against the $J-K$ colour for all the galaxies within 250 kpc of 3C 34 that have a K magnitude brighter than $K = 19$, that is, those bright enough to have their magnitudes measured to an accuracy $\lesssim 0.2$ mag. In this analysis, all magnitudes have been measured through a 4 arcsec diameter aperture, and corrected for galactic extinction using the extinction maps of Burstein & Heiles (1982). The three galaxies, 'a', 'b' and 'c', labelled in Fig. 1(a), are cross-referenced in Fig. 5; the galaxies labelled 'd', 'e' and 'f' in Fig. 5 lie outside the area shown in Fig. 1.

The near-infrared emission from these galaxies is dominated by their old stellar population and, out to a redshift $z \sim 1.5$, the infrared $J-K$ colour is a fairly strong function of the redshift of the galaxy. For passively evolving galaxies, the optical colour is also determined by the redshift of the galaxy, but any active flat-spectrum components (e.g. star formation, scattering, etc.) that may exist within the galaxies will make a large contribution to the optical and ultraviolet emission. Therefore, for galaxies of a given infrared colour, the optical f555W–f785LP colour can be used as an indicator of any activity within them. In Fig. 5 we display the colour track obtained by redshifting the spectrum of a standard elliptical galaxy (produced using the stellar synthesis codes provided by Bruzual & Charlot 1993, 1997), and assuming that there is no evolution of the stellar population.

It can be seen that the majority of the galaxies lie towards the upper right corner of this plot, close to the expected locus of a standard elliptical galaxy at the same redshift as 3C 34. This would be consistent with them being members of a cluster surrounding 3C 34 (McCarthy 1988), and shows that, at best, they are only passively evolving. A group of three galaxies, 'a', 'b' and 'd', possess the same infrared $J-K$ colours as the main group, suggesting that they may also be cluster galaxies. Their optical colours are, however, a magnitude bluer and so they must be optically active. Object 'a' is marginally the bluest of this set of galaxies. The difference in colour of object 'a' from the spectrum of a standard galaxy is apparent from a comparison of the images in Figs 2 and 3. The second bluer galaxy, 'b' (see Fig. 1a), lies close to the boundary of the radio lobe, and is elongated parallel to this transverse bow-shock, which may have some bearing on its bluer colour. The only other galaxy with $K < 19$ that lies projected within the radio lobe is the bright galaxy 'c' to the north of 3C 34 (see Fig. 1a); this lies on the edge of the radio tail emission, so would not be expected to be brightened. It is interesting to compare the optical activity seen in galaxies 'a' and 'b' with the observation of Röttgering et al. (1996) that, to account for the excess of companions along the direction of the radio axis in a sample of ultra-steep-spectrum radio sources, galaxies along the radio axis would have to be brightened in the optical waveband by up to 2 mag.

The third blue galaxy, 'd', is over 200 kpc from 3C 34, well away from the radio axis, and fairly symmetrical. Some other mechanism must be responsible for its colour. The two galaxies 'e' and 'f' which lie towards the lower left corner of Fig. 5 are likely to be foreground galaxies; they are 2 to 3 mag brighter in the f555W waveband than the other galaxies.

Based upon the optical, infrared and radio evidence, we conclude that it is likely that underlying the active flat-spectrum emission from object 'a' lies a galaxy at the same redshift as 3C 34.

3.3 The galaxy underlying object 'a'

It is reasonable to assume that object 'a' was an ordinary galaxy in the cluster containing 3C 34 before the radio source induced the flat-spectrum active component in some way. The infrared K image, which is relatively unaffected by the enhanced ultraviolet emission, shows the passively evolving old stellar population of the galaxy, whilst the f555W filter *HST* image is dominated by the optically bright regions corresponding to the induced active emission. Comparison of the locations of the optical and infrared emission indicates that the centre of the underlying galaxy lies in the gap between the two highly elongated emission regions.

We can use the K magnitude to normalize a fit of an old galaxy spectrum to the SED of galaxy 'a' at infrared wavelengths, using the stellar synthesis codes of Bruzual & Charlot (1993, 1997). We adopt a Scalo (1986) initial mass function with an upper mass cut-off at $65\,M_\odot$. To estimate the age of the galaxy, we first modelled the central cluster radio galaxy. The colours and images of this galaxy (Fig. 3) suggest that it is a passively evolving giant elliptical galaxy, and so we can fit the SED using a single population. The old stellar population is modelled as having an exponentially decreasing star formation rate with an e-folding time of 0.25 Gyr. It can be seen in Fig. 6(a) (solid line) that such a stellar population at an age of ~5.5 Gyr (corresponding to a formation redshift of $z_f \approx 10$) provides a good fit to the broad-band *HST* flux densities.

To model galaxy 'a', we assume that the underlying population has the same age as that of the central radio galaxy, that is, 5.5 Gyr: a good match to the infrared flux densities is provided using a galaxy mass of $1.65 \times 10^{10}\,M_\odot$ (see Fig. 6b, dotted line). This fit falls below the detected flux density at ultraviolet wavelengths, and so an

[2] Again, in the case of 3C 34 which possesses strong line emission, the f555W and f785LP flux densities have been corrected for line contamination.

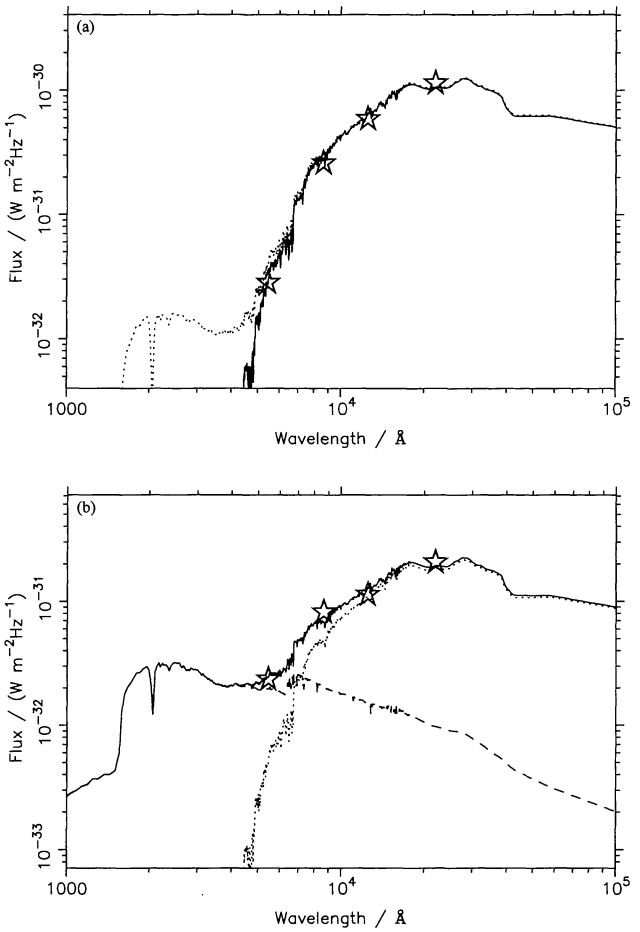

Figure 6. (a) (Top) Solid line – a fit to the SED of the galaxy associated with 3C 34, for a 5.5 Gyr old stellar population. Dotted line – addition of a 20 Myr old starburst (see Section 5). (b) (Bottom) Dotted line – a fit to the underlying old stellar population of galaxy 'a' using a 5.5 Gyr old stellar population. It can be seen that this falls short at ultraviolet wavelengths, requiring addition of a flat-spectrum component. Dashed line – the SED of a 1-Myr starburst observed 5 Myr after it ended (see Section 4.4). Solid line – a fit to the total SED of galaxy 'a' using the sum of the old stellar population and the starburst. The stars indicate the broad-band *HST* flux densities. These are corrected in (a) for strong line contamination. See text for more details.

active flat-spectrum component is required to account for the blue emission. This flat-spectrum component contributes about 80 per cent of the flux density detected in the f555W image. The total flux density measured using this filter through a 4 arcsec diameter aperture centred on 'a' is $(3.3 \pm 0.6) \times 10^{-32}$ W Hz^{-1}m^{-2}. Interestingly, the flux density within apertures tightly surrounding the three bright regions of emission in object 'a' amounts to $(2.75 \pm 0.4) \times 10^{-32}$ W Hz^{-1}m^{-2}, or about 85 per cent of the total. This is comparable to the predicted value, especially since a significant fraction of the light of the old galaxy will underlie these active regions and will therefore have been included. The conclusion that can be drawn from this is that these three bright components correspond to the active flat-spectrum emission regions.

A comparison of the flux density expected from the old stellar population in the infrared *J* band with that actually observed indicates that the flat-spectrum component makes a small (~15 per cent) contribution to the *J*-band flux density. This may account for the slightly disturbed nature of this image. Surprisingly, the same procedure indicates that the active emission should only contribute about 30 per cent of the light through the f785LP *HST* filter, with the old stellar population being responsible for the remaining 70 per cent; the *HST* image appears to be more dominated by extended aligned emission regions than by a passively evolving galaxy. At first sight this would seem to suggest that, instead of being a passive elliptical galaxy, the underlying galaxy itself must be somewhat extended along the radio axis. However, it must be remembered that the active emission regions have a much higher surface brightness than the more diffuse underlying galaxy, and also that a fraction of the flux density from a symmetrical galaxy would underlie the bright active emission regions.

To test whether this observation is consistent with the underlying galaxy being symmetrical, we attempted to remove the active component of the emission in the f785LP image, in order to see what remains. To achieve this, we used the f555W image as a template of where the active emission lies, and scaled it until the flux density of the flat-spectrum contribution at this wavelength matched the predicted flux density of that component in the f785LP observation. This scaled image was then subtracted from the f785LP image to remove the 30 per cent active emission in this filter; note that, owing to the presence of some galaxian component in the f555W image, this also involved unavoidable subtraction of some of the underlying galaxy light. The subtracted image was quite noisy, and so was convolved with a 0.3-arcsec Gaussian; this only smoothes the resultant image slightly, and has little effect upon either the image resolution or the qualitative nature of the resultant image.

This smoothed image is displayed in Fig. 7 as a contour plot overlying the f555W image. Although the resultant image does not follow a completely smooth galaxian profile, displaying three peaks of emission, these peaks are present only at low significance. It is also clear that this emission does not follow the extended blue emission seen in the grey-scale. The centre of this image lies directly over the centre of the *K*-band image, and if this image is convolved to the seeing of the infrared observations then its appearance matches exactly that of the *K* image.

It is not possible to discount the possibility that what we are actually observing here is a collision between two galaxies within the 3C 34 cluster. In this scenario, the various peaks within the galaxy in Fig. 7 would correspond to the central regions of the colliding galaxies, whilst the extended blue emission would be due to tails of gas resulting from the tidal interactions of the merging galaxies. However, the position of this merger directly along the axis of the radio source, coupled with the alignment of the tidal tails along the radio jet direction, makes this possibility highly unlikely.

More likely is that an ordinary galaxy does underlie object 'a', and that active emission has been induced in this in some way by the radio source. In the following sections we assume this to be the case, and discuss possible mechanisms for producing this aligned emission.

4 ALIGNMENT MECHANISMS

4.1 Scattering of quasar light by electrons or dust

According to some unification schemes of radio galaxies and quasars (Barthel 1989), these two populations of radio sources may arise from the same parent population viewed at different orientations. In this model, quasars have their radio axis orientated

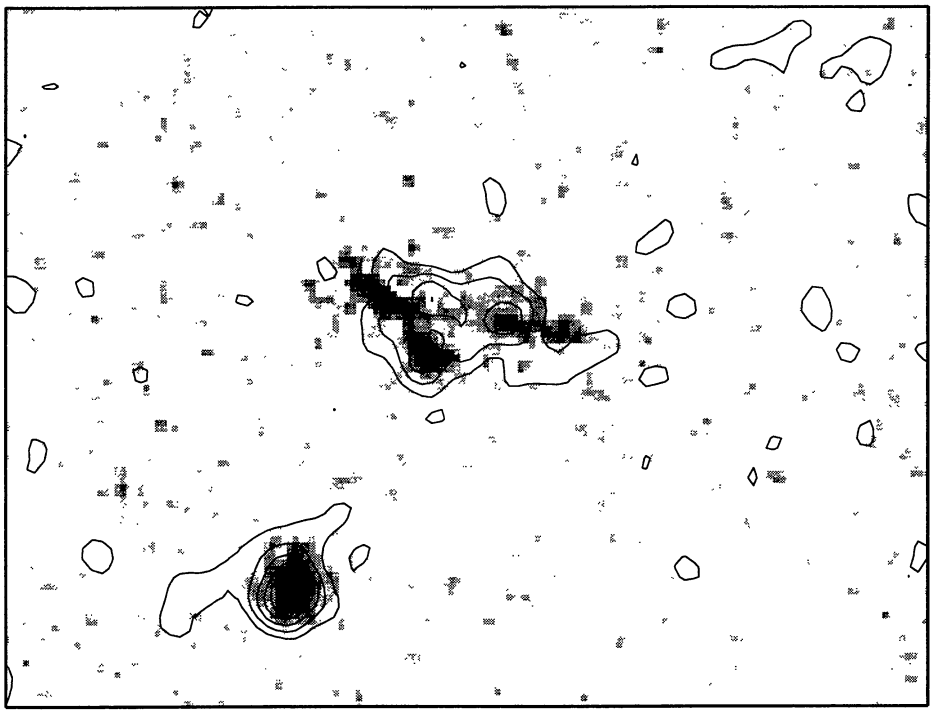

Figure 7. An image of the 'old stellar population' component of the f785LP image. This is created by scaling the f555W image (which is dominated by the active flat-spectrum emission), and subtracting it from the f785LP image to remove the predicted 30 per cent active flux from that image. The contours show the remaining flux, from the underlying galaxy. Relative to the first contour level, the contour levels are 1, 2, 3, 4, 5, 6. This image is not inconsistent with a smooth symmetrical galaxy underlying the active emission regions. The f555W image is plotted in grey-scale.

within about 45° of the line of sight, enabling us to observe their active galactic nuclei, whilst radio galaxies have their axis orientated towards the plane of the sky, and a torus of material obscures their central emission regions. In radio galaxies, scattering of the obscured quasar light by dust or electrons will produce polarized optical emission, which has been observed in many sources (e.g. Cimatti et al. 1996 and references therein). This scattering will occur not only along the radio jet direction, but from the whole cone within which the quasar light is emitted. Even if enhanced by the presence of dust or electrons associated with galaxy 'a', the morphology of the scattered light should track the underlying galaxy, rather than producing a linear feature.

If we assume that all of the flux from the 'active' regions of object 'a' is associated with scattered light, we can obtain a lower limit to the flux incident on this region from the quasar. We employ a similar method to that used by other authors (e.g. Eales & Rawlings 1990; van Breugel & Dey 1993).

The scattered luminosity, $L_{\rm scat}$, detected from object 'a' is related to the incident quasar luminosity, $L_{\rm Q}$, by

$$L_{\rm scat} \sim L_{\rm Q} \frac{R^2 \sin^2\theta}{D_{\rm proj}^2} f_{\rm c} \left(1 - {\rm e}^{-\tau}\right) G(\pi - \theta), \qquad (1)$$

where $L_{\rm scat}$ ($\sim 7.1 \times 10^{19}$ W Hz^{-1}sr^{-1}) and $L_{\rm Q}$ are measured in W Hz^{-1}sr^{-1}; R ($\approx$ 15 kpc) is the characteristic size of galaxy 'a'; $D_{\rm proj}$ ($\approx$ 120 kpc) is its projected distance from 3C 34; θ is the angle between the optical cone axis of the quasar emission and the line of sight; $f_{\rm c}$ is the covering factor of material within galaxy 'a', given by $f_{\rm c} \approx f_{\rm v}^{2/3}$, where $f_{\rm v}$ is the volume filling factor of the material; τ is the optical depth for scattering through galaxy 'a'; and $G(\theta)$ is the differential scattering cross-section of the scattering material. We adopt a value of $\theta = 90°$, meaning that the radio axis lies in the plane of the sky. This minimizes the amount of scattering required and is consistent with the symmetry of 3C 34.[3]

In the case of scattering by free electrons, $G(\theta) = \frac{3}{16\pi}\left(1 + \cos^2\theta\right)$, and the optical depth to scattering through galaxy 'a' is given by $\tau \sim n_{\rm e}\sigma_{\rm T} R f_{\rm v}^{1/3}$, where $n_{\rm e}$ is the number density of electrons and $\sigma_{\rm T} = 6.65 \times 10^{-29}$ m^2 is the Thomson scattering cross-section. The number density of electrons is obtained by averaging the mass of gas throughout the volume of the clouds within galaxy 'a'; $n_{\rm e} \sim M_{\rm gas}/(R^3 f_{\rm v} m_{\rm p})$, where $m_{\rm p}$ is the atomic mass.

Assuming that $L_{\rm Q} \sim 10^{23}$ W Hz^{-1}sr^{-1} (Osterbrock 1989), and noting that, since τ is small, $(1 - {\rm e}^{-\tau}) \approx \tau$, we can substitute these values into equation (1) and derive the mass of gas required to produce the observed scattering luminosity: $M_{\rm gas} \sim 2 \times 10^{11}$ M$_\odot$. This is much higher than estimates of the mass of warm ($T \sim 10^4$ K) emission-line gas within galaxies, which are in the range 10^7 to 10^9 M$_\odot$ (McCarthy 1993 and references therein), thus ruling out warm electrons as a possible scattering agent. Estimates of the hot X-ray gas masses in nearby galaxies lie in the range 10^8 to 10^{11} M$_\odot$ (Fabbiano 1989), with the upper end of the range corresponding to the most massive galaxies. The K-band magnitude of galaxy 'a' indicates that it is a fairly average galaxy (e.g. compare Figs 2d and 3d), and so it is extremely unlikely that it contains over 10^{11} M$_\odot$ of gas (cf. Section 3.3 where we derived a mass of 1.65×10^{10} M$_\odot$

[3]Many pieces of evidence suggest that 3C 34 lies more or less in the plane of the sky. (i) Jet candidates are identified in both lobes. (ii) The two lobes are roughly equal in length and, with the exception of the depolarization silhouette, also in Faraday depolarization. (iii) Both lobes show well-defined inner edges with a clear gap between the lobes corresponding to the position of the cluster core – if the source were at a significant angle to the plane of the sky, this gap would have been blurred.

of old stars in the galaxy). Scattering by hot electrons is therefore unlikely to play an important role in this object.

Dust scattering is more efficient than electron scattering in the ultraviolet waveband, since the scattering cross-section of dust particles is of the same order as the geometric cross-section. Following the same procedure as for electron scattering, and adopting values of $G(90°) \sim 0.05$ for the differential scattering cross-section, $a_d \sim 10^{-7}$ m for the radius of the dust grains, and $\rho_d \sim 3000\,\mathrm{kg\,m^{-3}}$ for their density (Whittet 1992), we derive an estimate for the dust mass required in galaxy 'a' of $M_{dust} \gtrsim 2.5 \times 10^7\,M_\odot$. For a galactic gas-to-dust ratio of about 150 (Whittet 1992) this give a total mass of gas in the warm phase (i.e. excluding the X-ray gas) of $M_{gas} \sim 4 \times 10^9\,M_\odot$. This, again, is a high mass of warm-phase gas compared with typical measured values, and compared with the mass of stars derived in Section 3.3. In addition, quasar light incident upon such a high mass of warm ionized gas would be expected to produce emission lines of sufficient strength to be observed in the spectrum (Fig. 4a). The absence of such lines therefore means that dust scattering is also unlikely to be of importance in object 'a'.

4.2 Inverse Compton scattering/optical synchrotron emission

Inverse Compton scattering and optical synchrotron emission should appear brightest at the peaks in the radio emission, rather than in a single elongated feature at a radio minimum. These mechanisms have been found to be important in some local sources, such as M87 (Biretta, Stern & Harris 1991), but are not generally found to be important in the powerful radio galaxies [see also van Breugel & Dey (1993) for 3C 285].

The flux density due to optical synchrotron emission can be calculated directly from the radio flux density by assuming a constant spectral index α:

$$\frac{f_{sync}(\nu)}{f_r(\nu_r)} \sim \left(\frac{\nu_r}{\nu}\right)^\alpha$$

which, in the region of object 'a', gives $f_{sync} \sim 1.4 \times 10^{-34}\,\mathrm{W\,Hz^{-1}m^{-2}}$. This will contribute less than 1 per cent of the flux density observed from this region. In practice the continuum spectrum is expected to steepen as the break frequency is passed (Hughes 1991), leading to an even lower limit to the level of optical synchrotron flux.

The contribution to the optical flux density from up-scattered microwave background photons can be calculated using the equations derived by Daly (1992a,b):

$$\frac{f_{ic}(\nu)}{f_r(\nu_r)} \sim 1.6 \times 10^{-12}\,\frac{(1+z)^{(1-\alpha)}}{\epsilon^{(1+\alpha)}}\,k\left[\frac{7.5 \times 10^{17}}{\nu}\,\frac{\nu_r}{178\,\mathrm{MHz}}\right]^\alpha,$$

where $f_{ic}(\nu)$ and $f_r(\nu_r)$ are the flux densities at the optical frequency ν and the radio frequency ν_r respectively; $\epsilon^2 = 0.092 B_\perp^2/(1+z)^4$ is a parametrization of the magnetic field in the lobe (measured in μG); α is the radio spectral index, $f_r(\nu) \propto \nu^{-\alpha}$; and k is a constant which depends upon α, having a value of 160 for $\alpha = 1$.

For the radio emission close to object 'a', $f_r \sim 1.5$ mJy at $\nu_r = 8.4$ GHz, $B \approx 10\,\mu$G, and $\alpha \approx 1$ (Johnson et al. 1995). Therefore, through the f555W filter, $f_{ic} \sim 2 \times 10^{-34}\,\mathrm{W\,Hz^{-1}m^{-2}}$, which is again much smaller than the observed flux density from object 'a'.

4.3 Nebular continuum emission

Dickson et al. (1995) recently suggested that a significant percentage of the ultraviolet flux from high-redshift radio galaxies may be associated with nebular continuum emission (free–free, free–bound and bound–bound interactions). If gas within galaxy 'a' were collisionally excited by shocks associated with the radio jet, these emission mechanisms would result in a morphology similar to that observed. The strength of nebular continuum emission is, however, strongly correlated with line strengths, and the failure to detect any emission lines indicates that this mechanism is unlikely to play a significant role in galaxy 'a'.

4.4 Young stars

Star formation induced by the passage of the radio jet through galaxy 'a' could give rise to a morphology similar to that observed. There is, however, a problem with the star formation hypothesis in that the flux of ionizing photons from the most massive stars in a newly formed stellar population should give rise to significant line emission. This problem can be circumvented by considering the ageing of a starburst population. In Section 3.1 we discussed the fact that the jet currently points at hotspot 's', and is no longer passing through galaxy 'a'. It is therefore reasonable to suppose that star formation may no longer be continuing in this galaxy. Indeed, if the period of star formation was a temporary phenomenon occurring only whilst the active hotspot region of the radio source was advancing through the galaxy [see Best et al. (1996) for a discussion of this model], then the age of the starburst can be estimated using radio spectral ageing arguments.

The radio spectrum is interpreted in terms of an ageing population of electrons, with the higher spectral index in the material further from the hotspots being due to the lower synchrotron break frequency in the older electron population. Assuming (i) a constant magnetic flux density, (ii) a standard power-law injection spectrum for the electrons, and (iii) that the electrons are isotropized on time-scales much shorter than their radiative lifetime, then the evolution of the break frequency with time is given by the equation (Pacholczyk 1970; Liu, Pooley & Riley 1992)

$$(\nu_T/\mathrm{GHz}) = 2.5 \times 10^3 \left[\frac{(B/\mathrm{nT})^{1/2}}{(B/\mathrm{nT})^2 + (B_{MWB}/\mathrm{nT})^2}\right]^2 (t/\mathrm{Myr})^{-2},$$

where ν_T is the break frequency, below which the spectrum is a power law, and above which it steepens; B is the magnetic field strength; $B_{MWB} = 0.315(1+z)^2$ nT is the equivalent magnetic strength of the cosmic microwave background radiation; and t is the spectral age of the electrons, that is, the time that has elapsed since they were last accelerated.

Blundell (1994) has estimated the strength of the magnetic field in 3C 34 using equipartition arguments (e.g. Alexander & Leahy 1987), and derived values of 0.5 to 1 nT in the inner regions of the radio lobes, that is, the regions closest to the host radio galaxy. These values are consistent with the estimates of a cluster magnetic field strength of 0.4 nT needed to produce the observed Faraday depolarization, if the depolarization is due to hot cluster gas of typical cluster density (Johnson et al. 1995). Blundell also fitted spectra to different regions of the source, and calculated the break frequencies at different locations. In the inner regions of the radio lobes these were typically 5 to 10 GHz.

Inserting these values into the above equation, the spectral ages of the oldest electrons, which are assumed to lie in the inner regions of the radio lobes furthest from the hotspots, are 9×10^6 to 3×10^7 yr, giving hotspot advance speeds of order $0.05c$. The distance between galaxy 'a' and the hotspot indicates that the starburst is observed about 6×10^6 yr after it was excited by the passage of the

radio jet through the galaxy. This corresponds roughly to the main-sequence lifetime of a 20-$M_\odot$ star, and so all stars of greater mass than this will have completed their evolution by the observed epoch.

Although infrequent in number, the strong dependence of stellar luminosity on mass means that these massive stars play a significant role in the starburst luminosity, especially at ultraviolet wavelengths. Returning to Fig. 6(b), we attempt to fit the excess ultraviolet emission required to account for the measured flux densities by adding a starburst population, observed 6×10^6 yr after it occurred, to the underlying galaxy SED. It is seen that a mass of 1.0×10^8 $M_\odot$ of young stars provides a good match to all of the observed data points. This corresponds to a star formation rate of about 100 $M_\odot$ per year during the 1-Myr burst.

In addition to dominating the starburst colour, the most massive stars, being the hottest, emit the vast majority of the photons with energies sufficient to ionize hydrogen and oxygen in these sources: the ionization potential of oxygen is 13.5 eV, nearly identical to that of hydrogen. In Fig. 8 we show how the number of photons emitted per second with sufficient energy to ionize hydrogen and oxygen decreases rapidly with age for the starburst considered above in galaxy 'a'. For comparison we also plot an estimate of the number of ionizing photons that would be intercepted by galaxy 'a' from an obscured quasar nucleus in 3C 34, assuming it to have properties typical of 3CR quasars at that redshift [i.e. $\sim 10^{54}$ ionizing photons per second (McCarthy 1993) emitted within a cone of opening half-angle 45°]. It can be seen that, at the distance of galaxy 'a' from the nucleus, the majority of its ionizing photons initially arise from the starburst, but the number of these decreases rapidly, falling by nearly a factor of 100 in 10^7 yr.

It is possible to estimate the emission-line flux that would be observed from galaxy 'a' if it absorbed all of the ionizing photons from the active nucleus. Using the simplest assumption, each ionizing photon will eventually produce one Lyα photon, and so the luminosity of Lyα due to the central AGN is about 9×10^{-20} W m^{-2}. Using a Lyα to [O II] 3727 ratio of 5, taken from the mean of a large number of radio galaxy spectra in which the emission lines are also excited predominantly by photoionization from the AGN (McCarthy 1988), this would mean that the [O II] line flux should be observed at about 1.8×10^{-20} W m^{-2}, which is between one and two times the noise level on the spectrum of galaxy 'a' (Fig. 4a).

In practice, not all of the ionizing photons will be absorbed, due to two factors: first, the covering fraction of the emission-line gas is likely to be less than one; secondly, the absorption rate is limited by the availability of neutral hydrogen atoms, which depends upon the recombination rate of the H^+ ions and electrons (e.g. Osterbrock 1989). If the emission-line gas is evenly distributed, producing a covering factor of unity, then the low hydrogen density dictates a slow recombination rate and limits the number of ionizations to $\sim 2 \times 10^{49}$ s^{-1}. For emission-line clouds with properties characteristic of those around high-redshift radio sources, that is $n_e \sim 10^8$ m^{-3} and a total mass of warm gas of $\sim 10^8$ $M_\odot$ (Heckman et al. 1991); the volume filling factor is only $\sim 10^{-5}$, meaning that the vast majority of the ionizing photons will pass through the galaxy unabsorbed. The larger number of ionizing photons associated with a newly formed starburst would produce line fluxes just detectable on the spectrum in Fig. 4(a). However, the decrease in ionizing photons that occurs by the age of $\sim 6 \times 10^6$ yr, at which this starburst is observed, produces a corresponding decrease in line fluxes, and reduces the expected line flux to below the noise level.

5 DISCUSSION

The results of Section 4.4 show that the lack of line emission from object 'a' is entirely consistent with an ageing starburst. Indeed, the rapid decrease of line emission with starburst age leads us to ask a different question: rather than ask why object 'a' does not show line emission, we should instead ask why Minkowski's object and the region 09.6 in the lobe of 3C 285 show so much, if they were formed by an interaction in a similar way to object 'a'. In the case of Minkowski's object, the object lies at the position where the radio jet disrupts, and is therefore likely to be the result of a relatively recent interaction. The knot 09.6 in the lobe of 3C 285, however, lies at a similar distance behind the hotspot to object 'a'. Van Breugel & Dey (1993) noted that it 'has an emission line spectrum typical of a starburst galaxy', but then suggested that it was an instantaneous starburst with an age of 70 ± 30 Myr, based on the spectral shape and the size of the 4000-Å break. Fig. 8 shows that, if this were the case, few high-ionization emission lines would be expected in the spectrum.

A reasonable fit to the spectrum of 09.6 can be obtained assuming a younger ($\lesssim$10 Myr) starburst involving about 10 per cent of the material from an older ($\sim$1 Gyr) galaxy. In this case, the size of the 4000-Å break is provided mainly by the older stars. This starburst age would also be more consistent with the radio spectral ageing of this source (Alexander & Leahy 1987), but even in this case it would be expected to have line emission as weak as that in galaxy 'a'.

In the case of 3C 34, the powerful jets were capable of driving through galaxy 'a', thereby inducing a rapid, short-duration burst of star formation with a highly elongated morphology tracking the passage of the jet. By contrast, the radio jet associated with 3C 285, which is roughly a factor of 100 lower in power than that in 3C 34, does not seem to penetrate the knot 09.6: the knot is fairly symmetrical apart from being edge-brightened, particularly in line emission, on the upstream side; the continuum is also bluest on the side facing the nucleus; the radio jet bends at a bright radio knot close to the point of impact with 09.6, indicating that the jet may have been disrupted and deflected by the knot, rather than passing through it. The interaction of the weaker jet in this source appears to have induced star formation only on the side of the knot that it originally struck, resulting in a significantly different physical situation as compared with that of galaxy 'a'. It is plausible that

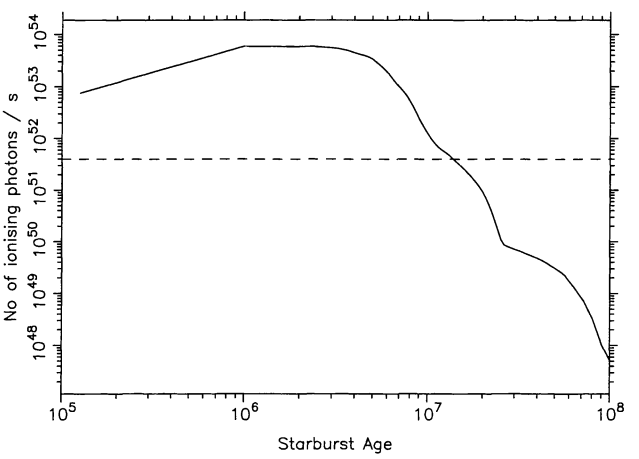

Figure 8. A plot of the number of ionizing photons against age of the starburst (solid line). The dashed line shows the constant level of ionizing photons arising from the AGN.

this weaker interaction may result in a less extreme but more prolonged starburst, with low levels of on-going star formation. Perhaps the bend in the radio jet at the knot near 09.6 results in momentum flux continuing to be incident upon the cloud, which may be responsible for its continued excitation.

It is interesting to compare our results with a recent observation by Cimatti et al. (1996) that a companion close to the radio galaxy 3C 324 ($z = 1.206$), and positioned along the radio axis, may plausibly be undergoing (or have very recently undergone) a burst of star formation at a rate of $70\,M_\odot\ yr^{-1}$. The similarity of this feature of 3C 324 to the situation in 3C 34 is striking.

The star formation rates suggested in these two cases can be compared with the values required to account for the aligned blue structures in the host galaxies of 3CR radio sources. Lilly & Longair (1984) accounted for the blue excess of high-redshift radio sources using star formation rates of 'several' solar masses per year for a duration of 10^7 to 10^8 yr, whilst Dunlop et al. (1989) suggested that about 1 per cent of the mass of the galaxy would need to be involved in the starburst. Each of these models predicts a comparable mass of young stars to the model presented here. Rees (1989) and Begelman & Cioffe (1989) have considered the star formation rates induced by radio bow-shocks expanding through a two-phase medium with reasonable filling factor and star formation efficiency, and have derived star formation rates of order $100\,M_\odot\ yr^{-1}$.

Our preferred interpretation for the recent history of 3C 34 is as follows.

(i) The radio jets were recently pointing towards hotspot 'n' in the western lobe, and the southernmost hotspot in the eastern lobe. The backflow of relativistic electrons from hotspot 'n' passed to the north of galaxy 'a'.

(ii) The radio jet passed through the halo of galaxy 'a' in the western lobe, and supersonic shocks associated with its passage induced a massive burst of star formation. The most massive stars died out within the few $\times 10^6$ yr between the onset of this starburst and the epoch at which we observe it, with the consequences that the colour of the starburst is redder than expected for a currently active star-forming region, and there are few ionizing photons to produce line emission.

(iii) Precession of the jets has given rise to a disconnection event in the western lobe, with the currently active hotspot 's' closer to the nucleus. The relativistic electrons continue to backflow through the evacuated region to the north of galaxy 'a'. In the eastern lobe, precession has resulted in the formation of new hotspots. The two radio knots lie along the current jet axis.

(iv) Shocks associated with the transverse expansion of the radio cocoon may have induced some star formation in other galaxies close to the radio axis, accounting for their blue optical colour.

In this model, the interaction of the radio jet with galaxy 'a' induces about 0.6 per cent of the mass of the galaxy to be converted into young stars in a time span of 1 Myr. To investigate the practicality of such a model, we can compare these predictions with the observations of a nearby system, the Cartwheel galaxy. In the Cartwheel galaxy, the passage of a companion through the spiral galaxy at small impact parameter has resulted in a rapidly propagating ring-shaped structure within the spiral disc (e.g. see Higdon 1995). Violent star formation is seen to be occurring at the shock front within this ring, and Kennicutt (1983) derived a star formation rate of $67\,M_\odot\ yr^{-1}$. This ring has been expanding for 300 Myr, and so a large fraction of the mass of this galaxy must have been involved in the starburst.

The passage of the companion through the Cartwheel galaxy is, in many ways, similar to the passage of the radio jet through galaxy 'a'. In galaxy 'a', the associated bow-shocks will be more powerful, and so will pass through the galaxy more quickly leading to the much shorter duration of the starburst. Despite the lower mass of this galaxy as compared with the Cartwheel, it is not unreasonable to expect that similar rates of star formation may occur.

Perhaps an even better comparison is that of nearby 'E + A' galaxies. These are galaxies which are dominated by a young stellar component, frequently involving up to 10 per cent of the galaxy mass, but which, like galaxy 'a', lack the emission lines characteristic of on-going star formation (e.g. Zabludoff et al. 1996 and references therein). It is thought that 'E + A' galaxies may be the result of violent galaxy interactions; the interaction of the radio jet with galaxy 'a' will produce a qualitatively similar result. Interestingly, 'E + A' galaxies have distinctive spectra dominated by strong Balmer absorption lines. Our spectroscopic data have neither the spectral resolution nor the signal-to-noise ratio necessary to detect these lines, but spectra of better signal-to-noise ratio at higher spectral resolution may provide direct proof of the existence, or otherwise, of an ageing starburst.

The separation of galaxy 'a' from the active galactic nucleus in this source suggests that the properties of this galaxy may not be typical of the aligned regions of the host radio galaxies. It possesses lower emission-line, scattered light and nebular continuum contributions, as compared with the extended emission regions in the radio galaxies. If, however, the radio jets are powerful enough to induce star formation over 100 kpc from the central engine, then the star formation process must also be of great importance in producing the aligned structures within the host galaxies.

One question that may be asked is why there is no evidence for star formation occurring within the host galaxy of 3C 34. The answer fits in remarkably well with our results from the study of the eight galaxies in the sample that lie within the redshift range $1 \lesssim Z \lesssim 1.3$ (Best, Longair & Röttgering 1996). The optical morphologies of these eight galaxies are seen to evolve strongly with radio size: small radio sources are composed of many bright knots of emission tightly aligned along the radio axis, whilst those with more extended radio emission contain only one or two bright components and generally have less extended optical emission.

Best et al. (1996) showed that this morphological evolution would be consistent with jet-induced star formation models whereby cold clumps of gas are induced to collapse and form stars as the radio components pass through the host galaxy, and these stars then evolve passively. The relatively short lifetimes of the most massive luminous stars, coupled with relaxation of the star-forming regions within the gravitational potential of the host galaxy, lead to a significant decrease in the starburst luminosity over the lifetime of the radio source.

3C 34 is one of the largest radio sources in our sample, and any star formation that occurred within the host galaxy will be about 2×10^7 yr old, meaning that the starburst will be well beyond its peak luminosity. By this age it is dominated, even in the rest-frame near-ultraviolet, by the much more massive old stellar population: addition of a $2 \times 10^8\,M_\odot$ starburst at this age has only a small effect on the infrared and optical spectral energy distribution (see Fig. 6a). If present, it may be responsible for the slight east–west extension seen at low significance in the f555W image (Fig. 3a), but our observations cannot distinguish whether or not such a population is present in this galaxy. Observations at 3000 Å, however, would easily distinguish whether an ageing starburst exists in older radio galaxies.

By contrast, star formation induced by the passage of the jet through galaxy 'a' is relatively recent: the structures bear a striking similarity to those seen within many of the smaller (younger) 3C radio galaxies. In addition, the significantly lower gravitational potential of galaxy 'a' will allow the strikingly aligned morphology of its young stars to remain visible for a longer period.

ACKNOWLEDGMENTS

This work is based on observations with the NASA/ESA *Hubble Space Telescope*, obtained at the Space Telescope Science Institute, which is operated by AURA, Inc., under contract with NASA. The National Radio Astronomy Observatory is operated by AURA, Inc., under cooperative agreement with the National Science Foundation. The authors thank Richard Saunders and Malcolm Bremer for kindly taking the spectrum of galaxy 'a', and Paddy Leahy for providing us with his radio map of 3C 34. We thank the referee for helpful comments. PNB acknowledges support from PPARC. HJAR acknowledges support from an EU twinning project, a programme subsidy granted by the Netherlands Organization for Scientific Research (NWO) and a NATO research grant.

REFERENCES

Alexander P., Leahy J. P., 1987, MNRAS, 225, 1
Barthel P. D., 1989, ApJ, 336, 606
Begelman M. C., Cioffi D. F., 1989, ApJ, 345, L21
Best P. N., Bailer D. M., Longair M. S., Riley J. M., 1995, MNRAS, 275, 1171
Best P. N., Longair M. S., Röttgering H. J. A., 1996, MNRAS, 280, L9
Best P. N., Longair M. S., Röttgering H. J. A., 1997, MNRAS, submitted
Biretta J. A., Stern C. P., Harris D. E., 1991, AJ, 101, 1632
Blundell K. M., 1994, PhD thesis, University of Cambridge
Brodie J., Bowyer S., McCarthy P. J., 1985, ApJ, 293, L59
Bruzual G., Charlot S., 1993, ApJ, 405, 538
Bruzual G., Charlot S., 1997, submitted
Burstein D., Heiles C., 1982, AJ, 87, 1165
Chambers K. C., Miley G. K., van Breugel W. J. M., 1987, Nat, 329, 604
Cimatti A., Dey A., van Breugel W., Antonucci R., Spinrad H., 1996, ApJ, 465, 145
Cox C. I., Gull S. F., Scheuer P. A. G., 1991, MNRAS, 252, 558
Daly R., 1990, ApJ, 355, 416
Daly R., 1992a, ApJ, 399, 426
Daly R., 1992b, ApJ, 386, L9
De Young D. S., 1989, ApJ, 342, L59
Dey A., Spinrad H., 1996, ApJ, 459, 133
Dickson R., Tadhunter C., Shaw M., Clark N., Morganti R., 1995, MNRAS, 273, L29
Dunlop J., Guiderdoni B., Rocca-Volmerange B., Peacock J., Longair M., 1989, MNRAS, 240, 257
Eales S. A., Rawlings S., 1990, MNRAS, 243, 1P
Fabbiano G., 1989, ARA&A, 27, 87
Fanaroff B. L., Riley J. M., 1974, MNRAS, 167, 31P
Garrington S. T., Conway R. G., Leahy J. P., 1991, MNRAS, 250, 171
Heckman T. M., Lehnert M. D., van Breugel W. J. M., Miley G. K., 1991, ApJ, 370, 78
Higdon J. L., 1995, ApJ, 455, 524
Hughes P. A., 1991, Beams and Jets in Astrophysics, Cambridge Astrophysics Series 19. Cambridge Univ. Press, Cambridge
Johnson R. A., Leahy J. P., Garrington S. T., 1995, MNRAS, 273, 877
Kennicutt R. C., 1983, ApJ, 272, 54
Laing R. A., Riley J. M., Longair M. S., 1983, MNRAS, 204, 151
Lauer T. R., 1989, PASP, 101, 445
Lilly S. J., Longair M. S., 1984, MNRAS, 211, 833
Liu R., Pooley G., Riley J. M., 1992, MNRAS, 257, 545
McCarthy P. J., 1988, PhD thesis, University of California, Berkeley
McCarthy P. J., 1993, ARA&A, 31, 639
McCarthy P. J., van Breugel W. J. M., Spinrad H., Djorgovski S., 1987, ApJ, 321, L29
Osterbrock D. E., 1989, Astrophysics of Gaseous Nebulae and Active Galactic Nuclei. University Science Books, Mill Valley, CA
Pacholczyk A. G., 1970, Radio Astrophysics. Freeman, San Francisco
Perley R. A., 1989, in Perley R. A., Schwab F. R., Bridle A. H., eds, ASP Conf. Ser. Vol. 6, Synthesis Imaging in Radio Astronomy. Astron. Soc. Pac., San Francisco, p. 259
Rees M. J., 1989, MNRAS, 239, 1P
Röttgering H. J. A., West M. J., Miley G. K., Chambers K. C., 1996, A&A, 307, 376
Scalo J. M., 1986, Fundam. Cosmic Phys., 11, 1
Scheuer P. A. G., 1982, in Heeschen D. S., Wade C. M., eds, Proc. IAU Symp. 97, Extragalactic Radio Sources. Reidel, Dordrecht, p. 163
van Breugel W., Dey A., 1993, ApJ, 414, 563
van Breugel W. J. M., Filippenko A. V., Heckman T. M., Miley G. K., 1985, ApJ, 293, 83
Whittet D. C. B., 1992, Dust in the galactic environment. IOP Publishing, Bristol
Williams A. G., Gull S. F., 1985, Nat, 313, 34
Zabludoff A. I., Zaritsky D., Lin H., Tucker D., Hashimoto Y., Shectman S. A., Oemler A., Kirshner R. P., 1996, ApJ, 466, 104

This paper has been typeset from a TEX/LATEX file prepared by the author.